Estimating dynamic brain functional networks using multi-subject fMRI data

Suprateek Kundu, *Emory University*
Jin Ming, *Emory University*
Jordan Pierce, *University of Georgia*
Jennifer McDowell, *University of Georgia*
Ying Guo, *Emory University*

Journal Title: NeuroImage
Volume: Volume 183
Publisher: Elsevier | 2018-12-01, Pages 635-649
Type of Work: Article | Post-print: After Peer Review
Publisher DOI: 10.1016/j.neuroimage.2018.07.045
Permanent URL: https://pid.emory.edu/ark:/25593/tkdf1

Final published version: http://dx.doi.org/10.1016/j.neuroimage.2018.07.045

HHS Public Access

Author manuscript

Neuroimage. Author manuscript; available in PMC 2018 December 01.

Published in final edited form as:

Neuroimage. 2018 December ; 183: 635–649. doi:10.1016/j.neuroimage.2018.07.045.

Estimating Dynamic Brain Functional Networks Using Multi-subject fMRI Data

Suprateek Kundu[a,1], **Jin Ming**[a], **Jordan Pierce**[b], **Jennifer McDowell**[b], and **Ying Guo**[a]

[a.]Department of Biostatistics, Emory University, 1518 Clifton Road NE, Atlanta, GA 30322, USA.

[b.]Department of Psychology, University of Georgia, 125 Baldwin Street, Athens, GA 30602, USA.

Abstract

A common assumption in the study of brain functional connectivity is that the brain network is stationarity. However it is increasingly recognized that the brain organization is prone to variations across the scanning session, fueling the need for dynamic connectivity approaches. One of the main challenges in developing such approaches is that the frequency and change points for the brain organization are unknown, with these changes potentially occurring frequently during the scanning session. In order to provide greater power tso detect rapidly evolving connectivity changes, we propose a fully automated two-stage approach which pools information across multiple subjects to estimate change points in functional connectivity, and subsequently estimates the brain networks within each state phase lying between consecutive change points. The number and positioning of the change points are unknown and learned from the data in the first stage, by modeling a time-dependent connectivity metric under a fused lasso approach. In the second stage, the brain functional network for each state phase is inferred via sparse inverse covariance matrices. We compare the performance of the method with existing dynamic connectivity approaches via extensive simulation studies, and apply the proposed approach to a saccade block task fMRI data.

Keywords

Brain functional connectivity; change point models; dynamic networks; fused lasso; graphical models; precision matrix estimation

1. Introduction

Neuroimaging studies have proved to be a pivotal tool for understanding the neurobiological basis of cognitive and behavioral outcomes in psychiatric studies, as well as for examining the pathophysiological mechanisms and the atypical brain development underlying mental disorders (Biswal et al., 1995; Greicius et al., 2003; Fox et al., 2005; Smith et al., 2009, among others). Traditional neuroimaging studies focus on identifying brain regions which are activated with respect to a certain task or outcome; however, in recent years, there has been a shift from region-based analyses to models involving brain networks. There have been some prominent findings which point towards the promise of brain functional network

[1]Please email the corresponding author at suprateek.kundu@emory.edu for any clarifications.

connectivity as an imaging biomarker which can be predictive of mental illnesses (Wang et al., 2007; Woodward and Cascio, 2015; Plitt et. al., 2015).

Many functional connectivity modeling approaches have been proposed, including independent component analysis (ICA) (McKeown et al., 1998,; Hyvarinen and Oja, 2000; Calhoun et al., 2001; Guo and Pagnoni, 2008; Beckmann and Smith, 2004, 2005; Guo, 2011), pairwise correlation analysis (Stam et. al., 2007; Suprekar et. al., 2008), partial correlation analysis (Salvador et. al., 2005) and sparse inverse covariance or precision matrix estimation (Huang et. al., 2009). Among those methods, precision matrix estimation was found to be one of the most successful approaches (Smith et. al., 2011; Wang et al., 2016), which can distinguish a true, direct functional connection from anapparent connection between two nodes, caused via confounding by a common third party node.

A key assumption which is common across all the aforementioned approaches is that the functional connectivity remains stationary during the whole scanning session. However, an increasing number of recent findings provide evidence on the dynamic nature of brain functional organization (Hutchinson et. al, 2012; Hellyer et. al, 2014). In particular, task-related imaging studies have shown that the brain networks will re-organize when the subjects undergo different modulations of the experimental tasks during the scanning session (Chang and Glover, 2010). Accurate detection and characterization of temporal variations in functional connectivity due to underlying neurobiological causes are not necessarily straightforward using the observed fMRI BOLD signals. Many non-neural related factors, such as low signal-to-noise ratio in the fMRI data, changing levels of non-neural noise resulting from background cardiac and respiratory processes and hardware instability, as well as variations in the BOLD signal mean and variance over time, can induce temporal variations (Hutchinson et. al., 2013; Lindquist et. al, 2014). Recently, studies are beginning to identify potential correlates of temporal variations in functional connectivity in simultaneously recorded electrophysiological data (Allen et al., 2013; Chang et al., 2013), behavior (Thompson et al., 2013), and disease status (Jones et al., 2012; Sakoglu et al., 2010). This recent evidence points to an underlying neuronal basis for temporal variations in functional connectivity which is linked with changes in cognitive and disease states, and provides a strong motivation for detailed investigation of dynamic brain connectivity.

Arguably, the most commonly used strategy for examining dynamic functional connectivity has been a sliding window approach (Allen et al., 2013; Chang and Glover, 2010; Handwerker et al., 2012; Jones et al., 2012; Sakoglu et al., 2010; Li et. al., 2013; Monti et. al., 2014; Liam et. al., 2015). While the sliding window technique is a valuable tool for investigating temporal dynamics of functional brain networks, there are some known limitations associated with this approach (Lindquist et. al, 2014) such as the choice of window length. In particular, a narrow window length will lead to a small number of time scans from which to estimate the brain networks in each state phase, potentially resulting in poor brain network estimates, whereas a large window length may overlook short term changes in the brain network. In addition, the sliding window techniques require secondary criteria to determine if variations in the edge structure are significant, which may not be straightforward to implement. For example, in a recent work by Hindriks et. al (2016), it was

shown that dynamic functional connections were almost impossible to detect using sliding-window correlations.

Dynamic functional connectivity is often conceptualized as a collection of state phases corresponding to various modulations in the brain, wherein the brain network remains relatively stationary within a state phase, but changes across different phases (Hutchinson et. al., 2013). This viewpoint can be suitably characterized by a change point model, which specifies the functional connectivity between two brain regions as a piecewise constant function over time with jumps at different change points (Cribben et. al., 2012, 2013; Lian et. al, 2015; Xu and Lindquist, 2015). Although existing change point models for dynamic functional connectivity have been somewhat successful in describing the temporal changes in the brain network, there are some existing challenges which involve the detection of rapidly evolving brain organization, that can change within as little as 30–60s (Sakoglu et al., 2010; Shirer et al., 2012; Jones et al., 2012). Such rapid fluctuations will divide the scanning period into a collection of narrow state phases, each containing only a few time scans from which to estimate the brain network, which is likely to violate an inherent assumption in existing approaches requiring a minimum number of scans between consecutive change points. A potential remedy is to pool information across multiple subjects as suggested by Hindriks et. al. (2016), who showed an increase in power for detecting brain connections by averaging over multi-subject data.

We propose a novel and fundamentally different change point model to detect temporal variations in the group level brain functional connectivity by combining data across multiple subjects. The proposed two-stage data-driven approach automatically estimates the number and locations of the change points from the data, as well as the time-varying brain network. The first stage estimates a connectivity metric at each time point based on multi-subject fMRI data and detects change points as shifts in the time series of this connectivity metric under a fused lasso approach. In the second stage, we use sparse inverse covariance matrix estimation to infer a distinct brain network for each state defined by the estimated change points. In addition, we introduce a subsampling scheme designed to reliably infer change points in the presence of aberrant subjects who may have different temporal dynamics compared to the majority of subjects, possibly due to behavioral differences or other causes. The proposed approach is expected to work best for task-based experiments involving multiple subjects who are engaged in the same task for a fixed time duration. A schematic illustration of the proposed approach is presented in Figure 1.

We evaluate the performance of the proposed method via extensive simulation studies involving several types of dynamic networks with rapidly evolving change points, and compare the performance with competing methods based on single subject, and multi-subject averaged data. We also apply our approach to a saccade block task data with alternate blocks of fixation and task, which involves rapidly evolving change points and aberrant subjects. For example, each block has only 10 time scans which lead to rapid changes in functional connectivity, and presents inherent challenges for an analysis based on single subject data. Moreover, there are several subjects who exhibit behavioral errors for one or more task blocks, which potentially reflect differences with the group level connectivity. Among other findings, our method is able to identify brain regions

supplementary eye fields, lateral and medial frontal eye fields, and cuneus as the most stable regions across the time varying network, which is consistent with previous evidence (McDowell et. al., 2008).

2. Materials and Methods

In this section, we introduce the two-stage approach for estimating dynamic functional connectivity. Suppose we are interested in studying the connectivity between p regions of interest (ROI) in the brain. From each ROI, the time-series of the blood oxygen level dependent (BOLD) signals is extracted to represent the neuronal activity within the ROI. To set notation, denote $\mathrm{y}_{it} = (y_{it1}, \ldots, y_{itp})$ as the vector of BOLD fMRI measurements obtained from the i-th subject at the t-th time point over the p ROIs, where $t = 1, \ldots, T, i = 1, \ldots, N$. To investigate the dynamic connectivity between the ROIs, we propose a two-stage approach, where the first stage identifies the change points for functional connectivity and the second stage estimates the brain networks appearing in various state phases which are time intervals separated by the change points.

2.1. Stage I: Change point estimation

To identify the change point in functional connectivity during the fMRI scanning, we first characterize the dynamic pattern in functional connectivity with a time course of a connectivity metric. Specifically, we propose to evaluate the time-dependent group functional connectivity between two nodes in the brain network by evaluating the correlations between the fMRI BOLD signals of these two nodes at each time point in the scanning session, averaged over subjects. The time courses of these pairwise correlations would then be used to identify the group level change points in functional connectivity. Here, we use pair-wise correlations instead of partial correlations as the connectivity metric due to the following reasons: (a) pair-wise correlations can be computed in a model-free manner, and they are computationally easier to estimate than the partial correlations, which requires the estimation of the precision matrix or fitting regression models; and (b) there is one-to-one correspondence between partial and pairwise correlations, and the time courses for these two types of correlations will have change points at exactly the same locations. We illustrate this concept in a toy example in Figure 2, which depicts changes in the time series of pair-wise correlations and corresponding partial correlations for a three node system. Given these reasons, we adopt pair-wise correlation as the connectivity metric for our change point estimation purposes in stage I. Subsequently in the second stage, we estimate the functional connectivity for each state phase (defined under the estimated change points), in terms of partial correlations under a graphical modeling approach involving sparse precision matrices.

2.1.1. Connectivity Metric—Suppose there are unknown change points denoted as $1 = a_0 < a_1 < \ldots < a_{K-1} < a_K < a_{K+1} = T$, which divides the scanning session into $K + 1$ distinct state phases, where the k-th tate phase consists of time points between a_{k-1} and a_k. The state phases represent time intervals between two consecutive change points where the brain network remains relatively stationary. Both the number and locations of change points

are unknown and are estimated as those points where the there is a change in the connectivity metric which is taken to be pair-wise correlations.

Let us denote the sample covariance matrices for time t as $\tilde{\Sigma}_t = \left(\rho_{t,rs}\right)_{r,s=1}^{p}$, and that for the k-th state phase as $\hat{\Sigma}_k$, where

$$\tilde{\Sigma}_t = \frac{\sum_{i=1}^{N}\left(\mathbf{y}_{it}-\bar{\mathbf{y}}_t\right)\left(\mathbf{y}_{it}-\bar{\mathbf{y}}_t\right)^T}{N}, \hat{\Sigma}_k = \frac{\sum_{a_{k-1}\le t\le a_k}\tilde{\Sigma}_t}{n_k}, t=1,\ldots,T, k=1,\ldots,K+1,$$

with n_k denoting the number of time scans in the k-th state phase $B_k = [a_{k-1}, a_k)$, and $\bar{\mathbf{y}}_t$ denoting the sample mean for time point t. The sample covariance matrices $\tilde{\Sigma}_1,\ldots,\tilde{\Sigma}_T$, represent the time series of sample pairwise correlation between the r-th and s-th ROIs which is averaged over all subjects, as $\tilde{\rho}_{1,rs},\ldots,\tilde{\rho}_{T,rs}$, where $\tilde{\rho}_{t,rs} = \tilde{\Sigma}_t(r,s)/\sqrt{\tilde{\Sigma}_t(r,r)\tilde{\Sigma}_t(s,s)}, r<s$ and $r,s=1,\ldots,p$. The sample pairwise correlations $\left\{\tilde{\rho}_{t,rs}, t=1,\ldots,T\right\}$ correspond to realizations for the time series of true pairwise correlations representing the time varying group level associations between pairs of regions/nodes in the brain. Let us denote the $p(p-1)/2$ dimensional vector of sample pairwise correlations at the t-th time point as $\tilde{\mathbf{r}}_t = \left\{\tilde{\rho}_{t,rs}: r<s, r,s=1,\ldots,p\right\}$ The time series of multivariate pair-wise correlations $\tilde{\mathbf{r}}_1,\ldots,\tilde{\mathbf{r}}_T$, characterize the dynamic connectivity patterns in the brain network. We detect temporal changes in functional connectivity by approximating the time series of multivariate pair-wise correlations via a piece-wise constant function under a fused lasso approach (Tibshirani et. al., 2004), which divides the scanning period into distinct state phases, such that the functional connectivity is constant within a state phase but changes across these phases. We elucidate the approach below.

2.1.2. A Fused Lasso Approach for Detecting Change Points in Brain Connectivity—

The fused lasso (Tibshirani et. al, 2004) is a generalization of the lasso (Tibshirani, 1996) approach which applies to settings where the observations have a natural ordering. The fused lasso can be used to detect changes in the mean of a naturally ordered set of observations by inferring spatial or temporal locations where jumps occur (Tibshirani and Wang, 2007). In our case, the set of ordered observations correspond to the time series of sample pairwise correlations, and one can examine the connectivity changes in the brain network by detecting shifts in this time series profile. To our knowledge, this is one of the first approaches to use the well established fused lasso method for detecting connectivity changes, although there is another recent work (Monti et. al., 2014) which uses a fused graphical lasso to estimate a distinct brain network at each time point. The approach by Monti et al. (2014) is based on sliding window correlations using single subject data, and is distinct from our approach which is focused on group level change point models.

To understand the application of the fused lasso approach for change point detection, let us first consider the special case when $p = 2$. In this case, the time series of univariate pairwise

correlations can be approximated via a piece-wise constant function under a fused lasso as follows

$$\min_{u \in \Re} \sum_{t=1}^{T} \left\| \tilde{\rho}_t - u_t \right\|^2 + \lambda \sum_{t=1}^{T-1} |u_{t+1} - u_t|, \quad (1)$$

where $\tilde{\rho}_1, \ldots, \tilde{\rho}_T$, are sample pairwise correlations as computed in Section 2.1.1, and $(u_1, \ldots, u_T)$ represents the piecewise constant approximation to the time series of pairwise correlations, with u_t denoting the assumed constant correlation during the interval $[a_t - 1, a_t)$. The optimization function in (1) is composed of two parts: (a) the first term captures the goodness of fit between the sample correlations $\tilde{\rho}$ and the assumed piecewise constant correlations u via a summed squared distance; and (b) the second term is the absolute difference between the piecewise constant function u between two consecutive time points, which equals zero is there is no jump ($|u_t - u_{t-1}| = 0$), and is greater than zero if there is a jump ($|u_{t-1} - u_t| > 0$). More generally, the second term aims to measure the number of jumps in the piecewise constant function, where the number and locations of the jumps are unknown and controlled by the sparsity parameter λ. When λ increases, this penalty will enforce many increments to become exactly zero, which will reduce the number of jumps and decrease the number of change points; on the other hand, a small value of λ will lead to a greater number of jumps. In summary, the optimization function in (1) aims to provide an adequate fit to the observed sample time series of correlations via a piecewise constant function with an unknown number of jumps that is controlled by the parameter λ.

In practical applications involving $p > 2$ ROIs in the brain, there are $p(p-1)/2$ distinct time series profiles of pair-wise correlations which are co-dependent on one another, and act in coordination to impact temporal variations in the brain functional connectivity. To tackle this issue, we present the following generalization of the original fused lasso in (1) to the case of multivariate time series of correlations, based on the approach in Vert and Bleakly (2010):

$$min_{\mathrm{u} \in \Re^{p(p-1)/2}} \sum_{t=1}^{T} \left\| \tilde{\mathrm{r}}_t - \mathrm{u}_t \right\|^2 + \lambda \sum_{t=1}^{T-1} \left\| \mathrm{u}_{t+1} - \mathrm{u}_t \right\|, \quad (2)$$

where $\left\| \mathbf{u}_{t+1,\cdot} - \mathbf{u}_{t,\cdot} \right\| = \sqrt{\sum_{m=1}^{p(p-1)/2} \left(u_{t+1,m} - u_{t,m} \right)^2}$, $\tilde{\mathbf{r}}_t$ is the vector of $p(p-1)/2$ sample pairwise correlations at time point t as computed in Section 2.1.1, and $\mathbf{u}_t \in \Re^{p(p-1)/2}$ represents the piecewise constant approximation to the multivariate time series at time point t. As in (1), the first term measures the error between the observed pair-wise correlations and the piece-wise constant function. The second term in (2) controls the increments between successive time points across the $p(p-1)/2$ pair-wise correlations, which collapses to zero when the multivariate time series does not change significantly successive between time points, and takes non-zero values corresponding to significant changes in functional connectivity. The penalty parameter λ in the second term influences the number of change points, in a manner similar to model (1). We denote the above approach as *connectivity*

change point detection which is abbreviated as CCPD. For a fixed value of λ, we can fit model (2) using the group lasso (Yuan and Lin, 2006), as described in the Appendix. In the next section, we describe a systematic procedure to choose the value of the penalty parameter λ.

2.1.3. Choice of the Penalty Parameter in CCPD—As pointed out in Section 2.1.2, the number of change points is determined by the penalty parameter λ, with a smaller value yielding a greater number of change points and vice-versa. Tibshirani and Wang (2007) proposed an estimate of λ based on a pre-smoothed fit of a univariate time series using a lowess estimator (Becker et. al, 1988). We adapt this approach for a multivariate time series to obtain an initial estimate for λ, and then propose some post-processing steps to tune this estimate and obtain change points.

Generalizing the approach in Tibshirani and Wang (2007) to the multivariate case, we apply lowess independently to each time-series of pair-wise correlations as a first step. Denote the smoothed fit as $\bar{\rho}_k = (\bar{\rho}_{k1}, \ldots, \bar{\rho}_{kT})$ for the k-th pair-wise correlation profile, $k = 1, \ldots, p(p-1)/2$. The fraction parameter in the lowess fit which controls the smoothness level, is chosen to be small so as to avoid oversmoothing which will cause difficulty in detecting potential change points. Then for each time series, we compute the first order differences $\delta_{kt} = \bar{\rho}_{kt} - \bar{\rho}_{k,t+1} t = 1, \ldots, T-1,$, followed by the median of $(\delta_{k1}, \ldots, \delta_{kT})$ denoted as μ_k, $k = 1, \ldots, p(p-1)/2$. Next, we compute the median of the absolute deviations $\{|\delta_{k1} - \mu_k|, \ldots, |\delta_{kT} - \mu_k|\}$, and denote it as Δ_k, $k = 1, \ldots, p(p-1)/2$. Finally, we compute an initial estimate for the penalty parameter given by

$$\lambda = \min_{k=1,\ldots,p} \{2\Delta_k + \sum_{t=1}^{T-1} |\delta_{kt}| 1(|\delta_{kt}| > 4\Delta_k)\}, \quad (3)$$

where $1(\cdot)$ is the indicator function. We then re-fit the fused lasso (2) under this chosen value of λ to obtain an initial estimate of the number of change points ($Kmax$) and their locations $\boldsymbol{\tau}^* = (t_1^*, \ldots, t_{Kmax}^*)$. The initial estimate for the number of change points is potentially inflated due to the choice of a small value of the lowess fraction parameter, and the manner in which λ was computed in (3). This is to ensure that we do not exclude true change points in the initial fit. In the next step we propose a screening criteria to exclude false change points in $\boldsymbol{\tau}^* = (t_1^*, \ldots, t_{Kmax}^*)$.

In particular, the screening criteria involves a post-processing step as follows. For each given subset of $k < Kmax$ change-points, we approximate the signals between the successive changepoints with the mean value of the points in that interval. Subsequently, we calculate the total sum of squared errors (SSE) between the set of real signals and these piecewise constant approximations to them. Though it may appear computationally intensive to do this for all subsets of $k < Kmax$ change-points, a dynamic programming strategy (Picard et. al, 2005) enables us to compute the subset of k change points having the minimum SSE from among all possible sets of $k < Kmax$ change points in $O(Kmax^2)$ time. Denote the minimum

SSE obtained from the subset of all possible k change points derived from the set $\boldsymbol{\tau}^*$ as SSE(k), and denote the corresponding locations of the change points as $\boldsymbol{\tau}_k^*$. Clearly, SSE(k + 1), will be smaller than SSE(k); however, after a certain point, adding an extra change-point will have no physical reality.

We determine the optimal number of change points by examining the curvature of the SSE curve as follows. First we normalize the minimum SSE scores $SSE(1), \ldots, SSE(Kmax)$ as $J_k = \frac{SSE(Kmax) - SSE(K)}{SSE(Kmax) - SSE(1)}(Kmax - 1) + 1$, where $J(1) = Kmax$ and $J(Kmax) = 1$ Then we compute the curvature of these normalized scores via discrete second derivatives as $\nabla_k = J_{k-1} - 2J_k + J_{k+1}$, and select the number of change points as $K = \max\{1 < k < Kmax : \nabla_k > 0.5\}$ such that the second derivative does not rise above a certain threshold on addition of further change points. The idea behind this approach is that if the curvature of the normalized SSE scores does not change beyond a certain value by adding an extra change point, then that will imply that the SSE does not reduce significantly, suggesting that no additional change points are required. In our experience based on extensive numerical studies, this approach is able to weed out any false change points included in the initial set of change points $\boldsymbol{\tau}^*$ and produces reliable estimates. We provide a summary of the above steps for estimating the number of change points in the form of Algorithm I in the Appendix.

2.2 Stage II: Brain Network Estimation based on Graphical Models

After estimating the change points in the stage I, the brain network within each state phase is estimated using graphical models, which estimates the strength of connections between p ROIs via partial correlations. The fMRI data will be pre-processed using standard procedures (Lindquist et. al., 2008) including de-trending and de-meaning. We also pre-whiten the observations to remove temporal correlations across scans. The pre-processed fMRI data are then assumed to be independent across scans, and distributed as a zero mean multivariate Gaussian distribution at each time point. Suppose $\boldsymbol{\tau}_K^* = \{a_1, \ldots, a_K\}$ are the estimated change points in Stage I. We propose the following Gaussian graphical model

$$\mathbf{y}_{it} \sim N\left(0,\ \Omega_k^{-1}\right), \text{if } a_{k-1} < t \leq a_k,\ k = 1, \ldots, K+1, \quad (4)$$

where $1 = a_0 < a_1 < \ldots < a_K < a_{K+1} = T$, and Ω_k is a sparse group level inverse covariance matrix for the k-th state phase ($k = 1, \ldots, K + 1$), from which one can derive partial correlations to estimate the brain network. We note that given the estimated change points in the stage I, there are $K + 1$ distinct brain networks encapsulated by $\Omega_1, \ldots, \Omega_{K+1}$. Model (4) specifies a group level change point model, where it is assumed that all the subjects in the group have the same transition points, which is a reasonable assumption for task based fMRI experiments. In the Section 2.3, we relax this assumption to identify and exclude aberrant subjects who have significant differences with the group level brain network.

The Gaussian graphical model in (4) enables us to infer brain networks in the form of sparse inverse covariance matrices $\Omega_1, \ldots, \Omega_{K+1}$ which cam be translated to graphs $G_1, \ldots, G_{K+1}$.

The graph G_k has the vertex set $V = \{1, \ldots, p\}$ corresponding to the p ROIs, and edge set E_k comprising all the edges in G_k corresponding to non-zero off-diagonal elements in Ω_k, $k = 1, \ldots, K+1$. The edges in E_k correspond to significant associations between pairs of ROIs in terms of partial correlations which can be computed as $\pi_{k,rs} = -\Omega_k(r,s)/\sqrt{\Omega_k(r,s)\,\Omega_k(s,s)}$, $r \neq s, r, s = 1, \ldots, p, k = 1, \ldots, K+1$. In other words, one can obtain the graph G_k, and hence the brain network for the k-th state phase, by studying the pattern of zeros in the sparse inverse covariance matrix Ω_k, $k = 1, \ldots, K+1$.

A popular method for estimating sparse inverse covariance matrices is the graphical lasso (Friedman et al. 2007) which is a penalized likelihood approach and can be thought of as an extension of the Lasso approach in regression settings. The graphical lasso operates by imposing a L_1 penalty on the off-diagonal elements of the inverse covariance matrix under a Gaussian likelihood, which results in zero off-diagonal entries corresponding to absent edges in the graph. We adopt the graphical lasso for brain network estimation, which estimates the sparse inverse covariance matrix for the k-th state phase as

$$\widehat{\Omega}_{k,\gamma} = \arg\min_{\Omega k}\left\{-\log\left(det\left(\Omega_k\right)\right) + tr\left(S_k\,\Omega_k\right) + \gamma\left|\Omega_k\right|_1\right\}, k = 1, \ldots, K+1, \quad (5)$$

where γ is the tuning parameter controlling for the sparsity of the graph, $\left|\Omega_k\right|_1 = \sum_{r,s}\left|\omega_{k,rs}\right|$ denotes the element-wise L_1 norm of Ω_k, S_k is the sample correlation matrix for all observations belonging to the k-th state phase which can be obtained directly from the sample covariance matrix $\hat{\Sigma}_k$ computed in Section 2.1.1. A higher value of the penalty parameter γ leads to sparser estimates of the inverse covariance matrix, and vice-versa. We obtain the solution in (5) corresponding to a grid of γ values, and choose an optimal value of γ which minimizes the BIC criteria computed as

$$BIC\gamma = \sum_{k=1}^{K}\left\{\sum_{t=1}^{T}\left(\mathrm{tr}\left(S_k\,\widehat{\Omega}_{k,\gamma}\right) - \log\left(det\left(\widehat{\Omega}_{k,\gamma}\right)\right)\right)1\left(a_{k-1} \leq t < a_k\right) + e_{k,\gamma}\log\left(n_k\right)\right\}, \quad (6)$$

where $e_{k,\gamma}$ is the number of edges under $\hat{\Omega}_{k,\gamma}$. We use the efficient algorithm developed by Friedman et. al. (2007) to implement the graphical lasso approach, which is available in the R package *glasso*.

2.3. A robust procedure for estimating group level dynamic connectivity

So far, we have assumed that all subjects share the same set of change points and have similar brain networks in each state phase. This assumption is theoretically reasonable for task-related fMRI studies where subjects engage in the same experimental paradigm. In practice, however, there may be some aberrant subjects whose neural activities do not properly align with the experimental tasks as expected. This may be reflected by the high behavioral error rates in their task performance. For example, in our study with saccade trails, few subjects have slower response times and a lower number of correct responses due

to behavioral errors, but the majority of subjects have negligible errors implying consistency in the behavioral response. It is reasonable to assume that the brain connectivity for these aberrant subjects will exhibit systematic differences with the group level brain network. Hence, we would ideally like to identify and exclude these unknown aberrant subjects from our change point and brain network estimation, while retaining the other typical subjects for inferring group level connectivity.

We propose an approach that can provide reliable estimates of dynamic connectivity patterns in the presence of aberrant subjects. The proposed approach is based on a sub-sampling scheme. We randomly select a sub-sample of pre-specified size by excluding a small subset of subjects, and compute the change points based on this sub-sample using the methods in Section 2.1. This procedure is then repeated multiple times with distinct sub-samples, and a set of change points is computed for each sub-sample. Once this process is completed, the final change points are estimated as those which appear most frequently across all the sub-samples. The justification for this approach lies in the fact that change points which are supported by the majority of the subjects in the dataset, will be detected more frequently across multiple sub-samples, and any fallacious change points which may show up in one or more sub-samples due to the influence of aberrant subjects will be eliminated through this process. By choosing to work with multiple subsamples having a reduced sample size, our goal is to ensure a robust change point estimation by reducing the impact of the aberrant subjects. The change points estimated under this approach represent group level dynamics in the brain network, after excluding a small group of aberrant subjects whose functional connectivity changes do not properly align to the experimental task.

In order to identify aberrant subjects, we compute the sparse inverse covariance matrix as in Section 2.2 using the estimated change points, independently for each subject. This essentially reduces to computing the estimate in (5) where the covariance matrices S_1, …, S_{K+1}, are computed based on single subject data. The individual BIC scores using single subject data are then computed using (6), and those who have BIC score above a certain threshold are identified as aberrant subjects, since a higher BIC score implies the inadequacy of the model fit under the estimated change points. These identified aberrant subjects are then excluded, and the group level dynamic brain network is computed using the remaining typical subjects, under the methods in Section 2.2.

3. Result

3.1. Simulation Sstudies

3.1.1. Simulation Set-up—We conducted a series of simulation studies to examine the performance of our approach in terms of change point detection, and brain network estimation. We generate data sets which include both typical subjects (N=55) having common change points, and also aberrant subjects (N=5) who have subject-specific change points. The data was generated under a Gaussian graphical model (4) containing four state phases corresponding to closely located change points.

We evaluated the performance of the proposed method for a range of networks with different characteristics. In particular, we consider the brain networks derived from four different

types of graphs: (a) Erdos-Renyi random graphs (Erdos and Renyi, 1959) was generated for the first state phase using the same probability for all connections (0.15), while the networks for the subsequent state phases are obtained by flipping a subset of edges (adding an edge if there was no edge, and deleting an edge if there was one) in the graph corresponding to the previous state phase; (b) Erdos-Renyi random graphs (Erdos and Renyi, 1959) were generated independently for each state phase; (c) scale-free graphs were generated independently for each state phase using the preferential attachment model of Barabasi and Albert (1999); and (d) small-world random graphs, obtained using the Watts and Strogatz (1998) model, were generated independently for each state phase. The random graphs in (a) mimic the time varying brain networks which retain certain connections between consecutive state phases, but discard others, while the random graphs in (b) represent a random network setting that is commonly seen in various types of data and has been widely studied. On the other hand, the scale-free and small-world networks in (c) and (d), are motivated by the characteristics of real life brain networks derived from fMRI data.

Given the graph, the corresponding precision matrix was computed by fixing off-diagonals to zero for absent edges, and randomly generating elements from $U(-1, 1)$ corresponding to important edges. The diagonal elements are then rescaled appropriately to yield a diagonally dominant structure which ensures positive definiteness. The simulated brain network and the corresponding precision matrix was constant for all time scans within a state phase but they were different across the state phases. The data was generated independently for all subjects using a Gaussian graphical model characterized by the precision matrices generated in the above manner. All the typical subjects were assigned the same time varying connectivity, while the aberrant subjects had distinct change points and brain networks simulated in the manner discussed above.

For each type of graph, we then considered four combinations of the number of nodes (p) and total number of time scans (T), i.e. (p, T) = (10, 200), (20, 200), with change points as 40,80,140, and (p, T) = (10, 300), (20, 300), with change points as 40,115,175. For the random graph in (a), we generated 12 scenarios. Scenarios 1–4 involve the above four combinations of (p, T); scenarios 5–8 are similar to scenarios 1–4 but involve mean changes at the change point locations along with connectivity changes; whereas scenarios 9–12 are similar to scenarios 1–4, but involve the presence of random spikes in the time series. These different cases reflect practical issues encountered in fMRI data. We also generated data under the Erdos-Renyi graphs (Scenario 13–16), small world networks (Scenario 17–20), and scale free networks (Scenario 21–24), corresponding to the four (p, T) combinations mentioned above. We generate 100 replicates for each simulation scenario and report performance metrics averaged over these replicates.

3.1.2. Performance Metrics—We evaluate the performance of the proposed method for change point detection as well as network estimation. To assess the performance in terms of change point estimation, we report the proportion of change points that were detected correctly across replicates. In order to assess graph estimation performance, we compare the estimated and the true network at each time point in terms of sensitivity and specificity, and then average these metrics across time points. Sensitivity represents the power to detect true connections and is computed as the proportion of true connections detected under the

approach, while specificity is equivalent to 1-false discovery rate (FDR), and is computed as the proportion of missing connections which are correctly classified as absent. We also present receiver operating characteristic (ROC) curves for graph estimation for the first four simulation cases, which plots the sensitivity versus 1-specificity levels for a series of graphs estimated by varying the penalty parameter γ in (5). A higher area under the ROC curve implies more accurate graph estimates across all values of the penalty parameter, with higher sensitivity and specificity levels. Finally, we also examine computation times under our method.

We compare our approach with dynamic connectivity regression (DCR) proposed by Cribben et. al. (2012), which divides up the scanning session into piecewise stationary segments using a BIC criteria involving hypothesis testing, and computes the graph for each such segment using the graphical lasso. The sensitivity and specificity under the estimated graphs for each segment are computed, and these are averaged to report a point estimate. The software for implementing this approach is available in the author's website. We also compare with the sliding window technique, where we obtain local estimates of the covariance matrices by downweighting time points far away using a kernel function $K_h(i, j) = I(|i - j| \leq h)$ (Monti et. al, 2014). Here, $I(\cdot)$ is an indicator function, and $K_h(i, j)$ represents the weight given to time point j when computing the local covariance matrix at time point i corresponding to window length h. Given the kernel function, the local mean at the timepoint i is $\bar{\mathbf{y}}_{i,SL} = \sum_{j=1}^{T} K_h(i, j)\mathbf{y}_i / \sum_{j=1}^{T} K_h(i, j)$, and the local covariance matrix is $S_{i,SL} = \Sigma_{j=1}^{T} K_h(i, j)(\mathbf{y}_i - \bar{\mathbf{y}}_{i,SL})(\mathbf{y}_i - \bar{\mathbf{y}}_{i,SL})^T / \Sigma_{j=1}^{T} K_h(i, j)$. We then average these local covariance matrices for each time point across all subjects, and use them to obtain group level estimates for the graph at each time point under the graphical lasso method. We compute the sensitivity and specificity under the estimated graphs at each time point, and average across them. We present the sliding window results under window lengths of 10 and 50. We note that the DCR results are based on single subject analysis, while the sliding window analysis in this article relies on multi-subject averaged data.

3.1.3. Simulation Results—From Table 1, we see that the proposed approach is able to detect the true change points for all scenarios, even in the presence of aberrant subjects and spurious patterns involving spikes and mean changes. On the other hand, the DCR approach performs poorly, often missing change points altogether for most subjects. In terms of graph estimation, the proposed approach has sufficiently high sensitivity (between 0.85–0.90) across all scenarios, which means it can efficiently estimate true connections in the graph, as well as high specificity (between 0.90 to 0.98), implying adequate control over false discoveries. Moreover, it is evident that the DCR reports extremely low sensitivity levels, which is potentially a direct consequence of poor change point estimation. In particular, the fallacious change point detection under DCR introduces false time scans belonging to another state phase when estimating the graph corresponding to a particular state phase, which leads to poor power for detecting the true connections. The sliding window approach having a window length of 10, results in comparable specificity levels for the 12 scenarios involving random graphs, but lower specificity for the other scenarios. Moreover the sensitivity levels of the proposed approach are uniformly and significantly higher for all

cases. Finally, the sliding window results for a window length of 50 result in sensitivity and specificity levels which are both uniformly and significantly lower than the reported levels under the proposed approach. These results imply that the choice of the window length is crucial for obtaining meaningful results under the sliding window approach. We also experimented with other window lengths (results not presented here), but discovered that the sliding window results were consistently inferior to the proposed approach.

The ROC curves for the first four simulation cases are presented in Figure 3. It is clear that the ROC curve under the proposed approach demonstrate better performance compared to the ROC curves for the other competing approaches, with greater sensitivity and specificity across all values of the tuning parameter. Further, the sensitivity of the proposed approach rapidly rises to one, for low levels of false discovery, which suggests the ability of the proposed method to correctly detect true edges while controlling for false discovery rates. The ROC curves for the other simulation cases convey similar information regarding the relative performance, although they are not presented here due to space constraints.

We also observed that the performance of DCR improves when the distance between change points is substantially large (100 or more), but the method performs poorly when the change points are closer together, which is often the case in practice (Sakoglu et al., 2010; Shirer et al., 2012; Jones et al., 2012). We conjecture that the poor performance of DCR in scenarios involving closely spaced change points is due to the fact that DCR is based on single subject data analysis. In comparison, the proposed approach is able to accurately detect closely spaced change points, by pooling data across multiple subjects under the assumption of common change points across a majority of subjects in the sample.

We performed additional simulations for scenarios 1–4, which suggested that the sensitivity and specificity levels rise to one under the proposed approach when the sparsity of the true graph is further increased, or if the number of time points between consecutive change points increase. We also examined the effect of varying the number of aberrant subjects on the numerical performance. Our results indicate that (a) the graph estimation under the proposed approach improves even further when there are no aberrant subjects in the sample; and (b) the proposed approach is able to detect all the change points accurately as long as the number of aberrant subjects does not exceed one third of the total sample size; however the graph estimation becomes less accurate in these cases.

From our numerical experiments, we expect that the proposed approach will work well in task based fMRI experiments, where the number of aberrant subjects is expected to be limited. From Table 2, we see that the proposed approach has a reasonable computational time. From our experience in simulations in the presence of aberrant subjects, the proposed approach is readily scalable to more than a hundred nodes. Further, the approach can be scalable to even larger number of nodes in the absence of aberrant subjects. In general the scalability of the approach is inversely proportional to the number of aberrant subjects assumed to be present in the sample.

3.2. Experimental Data for Saccade Trials

3.2.1. Saccade Trial fMRI data and pre-processing steps—We look at a block task data involving a saccade fMRI trial at the University of Georgia, Athens. Data was collected from 35 right-handed, healthy participants (mean age = 19.5 years, SD = 3.7; 10 males), who experienced no current major psychiatric disorders or substance abuse, had no metal implants, and had normal or corrected-to-normal vision (via self-report), as described in Pierce and McDowell (2016). Participants completed a saccade blocked task which consisted of repeating 20 second blocks (10 scans) of a) fixation (9 blocks), b) pro-saccade trials (4 blocks), and c) anti-saccade trials (4 blocks). The blocks were arranged as fixation followed by prosaccade, then fixation followed by antisaccade, and this sequence was repeated several times such that the total number of scans combining all the task blocks was 170, and the total scan time was 5 minutes and 48 seconds. All stimuli consisted of a 1 degree gray shape presented on a black background (Pierce and McDowell, 2016). During fixation a cross appeared in the center of the screen; subjects were asked to look as quickly and accurately as possible towards the peripheral stimulus for prosaccade task and towards opposite location of the stimulus, same distance from the center, for the anti-saccade task.

Participants attended an initial screening session, where they completed demographic surveys and performed twenty practice trials of mixed prosaccades and antisaccades. Those who met inclusion criteria were scheduled for a subsequent MRI session. A high-resolution structural scan was obtained first for each participant, followed by several functional scans (only one of which is reported here). Stimuli were displayed using Presentation software (Neurobehavioral Systems, Albany, CA) and a dual mirror system attached to the head coil that allowed a participant to view a projection screen at his/her feet and researchers to monitor the participants eye. Right eye pupil position was sampled at 60 Hz (IView X MRI-LR system, SensoMotoric Instruments, Germany) and recorded for off-line analysis. Before beginning the saccade tasks, eye position was calibrated using IViews 5-point calibration and an in-house horizontal calibration.

MR images were collected on a 3T GE Signa Excite HDx system (General Electric Medical Systems, Milwaukee, WI) at the University of Georgia Bio-Imaging Research Center. A high-resolution anatomical image was collected using a T1-weighted 3D FSPGR sequence (echo time = 3 ms, flip angle = 20 degrees, field of view (FOV) = 240 mm × 240 mm, matrix size 256 × 256, 150 axial slices, in-slice resolution = 0.94 × 0.94 mm, slice thickness = 1.2 mm, scan time=6 minutes and 32 seconds). The functional scans were collected using a $T2^*$-weighted gradient echo EPI sequence (echo time = 30 ms, repetition time = 2000 ms, flip angle = 90 degrees, FOV =220 mm × 220 mm, matrix size = 64 × 64, 33 interleaved oblique slices aligned with the AC-PC plane in-slice resolution = 3.4 × 3.4 mm, slice thickness = 4 mm, and 4 dummy volumes for magnet stabilization).

Eye position data were analyzed using custom scripts written in MATLAB (MathWorks, Natick, MA). Trials were manually scored for initial direction of response (eye movements with velocities surpassing 20 degree/sec were classified as saccades). Trials with no response, blinks at stimulus onset, anticipatory saccades (faster than 90 ms latency or during the gap window), or with insufficient data quality due to loss of pupil tracking were

excluded from further analysis. Pre-processing of functional MRI data was performed using the AFNI software package (Cox, 1996, 2012) and included: slice-timing correction, volume alignment, resampling to 4 mm^3 voxel grid, spatial standardization to a Talairach template, spatial smoothing (4 mm full width-half maximum Gaussian kernel), and voxel-wise scaling to a mean of 100. Regions of interest (ROIs) were identified using 6 mm spheres centered on coordinates from a previous saccade study (Dyckman et. al., 2007) that included supplementary eye fields (SEF), lateral and medial frontal eye fields (FEF), prefrontal cortex (PFC), inferior frontal cortex (IFC), precuneus, cuneus, inferior parietal lobule (IPL), middle occipital gyrus (MOG), striatum, and thalamus. The average preprocessed time series then was extracted from each ROI for each participant, for estimating the dynamic brain functional connectivity.

We deleted the first four task blocks (fixation-pro-fixation-anti) from our analysis, in order to exclude data from the high variability blocks where subjects were still familiarizing themselves with the task. We also excluded data from the anti-saccade blocks due to high error rate and variability across subjects associated with this task, which is potentially indicative of varied brain states during these trials. Here, error rate is defined as the number of trials with an initial saccade in the incorrect direction divided by the total number of scoreable trials. We then applied the proposed approach to detect change points and estimate dynamic networks based on blocks associated with the pro-saccade task and fixation.

3.2.2. Analysis Results—Our analysis detected changes in the saccade network at the beginning of the pro-saccade and fixation blocks which is consistent with the experiment design. In addition, we also detected change points in the middle of blocks two fixation blocks and one pro-saccade block. This results implies that the brain networks tend to be stationary during the majority of the task and rest phases, however there could be occasional network changes within a task or rest block. We conjecture that these changes near the middle of the blocks are potentially due to anticipation of the fixation block at the end of a task block, and vice-versa.

To characterize how the brain network during a saccade task shifts during pro-saccade and fixation blocks, we examined the partial correlations between all pairs of ROIs during each brain state between the change points. Then, we identified those connections that were relatively stable (i.e., present in at least 50% of the brain states) across both pro-saccade and fixation blocks, exclusively for pro-saccade blocks, exclusively for fixation blocks, or neither block. These connections are depicted in Figure (4). The analysis revealed that there was a higher number of stable connections for pro-saccade (29) compared to fixation blocks (17). The SEF, medial FEF, and cuneus had the largest number of stable connections during task or both blocks, while the thalamus had a high number of connections exclusively during the task block. Moreover, there were only three connections (IFC-SEF, IFC-IPL, and IPL-MOG) that were present at fixation that did not also occur during the pro-saccade task. Striatum and MOG had the fewest stable connections across the scanning session.

This pattern of results implies that SEF, FEF, and cuneus are core regions in the saccade network and that they maintain functional connectivity with multiple nodes in the network throughout the task as well as during intervening fixation blocks. These regions are known

to be critical for visual processing and saccade generation (McDowell et al., 2008) and the number of consistent connections identified here demonstrates their relevance to the saccade network over time. The thalamus, in contrast, was connected to the saccade network specifically during the pro-saccade task blocks, indicating a dynamic role in ocular motor control that may be interrupted during non-active blocks. Striatum and MOG have also been reported during saccade activation studies, yet showed limited stable connections to other saccade ROIs here. Interestingly, the striatum was connected to the thalamus, while MOG was connected to the cuneus, during all the analyzed brain states. This suggests that these two regions are more functionally distant in the saccade network and their interactions may be mediated largely by other, more central nodes. Overall these findings support activation studies of saccade tasks on the role of many of these ROIs in the ocular motor network, as well as providing new insight into how these regions functionally interact over the course of task and fixation blocks in a saccade paradigm.

4. Conclusion

We have proposed a fundamentally novel approach for detecting temporal changes in the brain functional connectivity, and for estimating a time varying brain network based on multi-subject fMRI data. By pooling information across subjects, the proposed approach has major advantages over existing methods. It provides more reliable estimation of group-level dynamic connectivity in task-related fMRI studies. In particular, our method provides greater power for detecting rapid changes in functional connectivity, that can otherwise be challenging to detect using a single subject analysis. We further propose a robust procedure for accurately detecting the true change points even in the presence of aberrant subjects, who demonstrated significantly differently dynamics in connectivity from the group mostly because their neural activity was inappropriate registered to the experiment tasks. We show through extensive simulation studies that the proposed method had significantly superior performance to methods based on a single subject analysis, and another approach based on sliding window correlations averaged over multiple subjects. The proposed method accounts for individual level differences by identifying and eliminating aberrant subjects who exhibit significant differences in the dynamic brain functional connectivity compared to the group, and is expected to work well in settings involving a limited number of aberrant subjects, such as in task based fMRI experiments. We apply the method to a block task saccade trial, where it successfully detects temporal variations in the brain functional connectivity, and identifies several important regions and connections which have been previously linked with saccade circuitry.

The proposed approach assumes that the fMRI data is available on all all subjects at the same set of time points, such that measurements for each scan can be aligned across subjects. Based on this assumption, our approach is mainly applicable for estimating group-level dynamic connectivity in task-related fMRI studies where subjects are imaged under the same experimental paradigm.

Acknowledgements

Research reported in this publication was partially supported by the National Institute Of Mental Health of the National Institutes of Health under Award Number ROI MH105561 and R01MH079448. The content is solely the responsibility of the authors and does not necessarily represent the views of the funding agencies involved.

Appendix

Computational Details for Fitting CCPD

We fit model (2) using a group lasso approach, after suitable transformation of variables. Denote $\boldsymbol{\alpha}_0 = \mathbf{u}_1$, and the increments as $\boldsymbol{\alpha}_i = u_{i+1} - u_i, i = 1, \ldots, T-1$. Then we have, $\mathbf{u}_1 = \boldsymbol{\alpha}_0$, and $u_i = \boldsymbol{\alpha}_0 + \sum_{l=1}^{i-1} \alpha_l$ for $i = 2, \ldots, T$. Further let $\tilde{R}$ denote the $T \times p$ matrix having $\tilde{r}_t$ as the t-th row ($t = 1, \ldots, T$), and A denote the $(T-1) \times p$ matrix having $\boldsymbol{\alpha}_k$ as the k-th row ($k = 1, \ldots, T$). Further denote X as the $T \times (T-1)$ matrix having elements (k, l) as one if $k > l$, and zero otherwise. It can be shown that the equation (2) may be re-written as

$$min_{A \in \Re^{(T-1)\times p}, \boldsymbol{\alpha}_0 \in \Re^p} \left\| \tilde{R} - XA - 1_T \boldsymbol{\alpha}_0 \right\|^2 + \lambda \sum_{t=1}^{T-1} \left\| \boldsymbol{\alpha}_t \right\| \qquad (7)$$

$$= \min_{A \in \Re^{(T-1)\times p}, \boldsymbol{\alpha}_0 \in \Re^p} \left\| \tilde{R}_c - X_c A - 1_T \boldsymbol{\alpha}_0 \right\|^2 + \lambda \sum_{t=1}^{T-1} \left\| \boldsymbol{\alpha}_t \right\|,$$

where X_c and $\tilde{R}_c$ are obtained from X and $\tilde{R}$ respectively, after centering each column. The equality in (7) can be obtained by substituting $\boldsymbol{\alpha}_0 = (\tilde{R} - XA)1_T$. Equation (7) can be solved using the group lasso approach in Yuan and Lin (2006), for which existing R packages are available.

References

1. Allen E, Damaraju E, Plis SM, Erhardt E, Eichele T, Calhoun VD, 2012 Tracking whole-brain connectivity dynamics in the resting state. Cereb. Cortex bhs352
2. Barabasi AL, Albert R, 1999 Emergence of scaling in random networks. science 286(5439), 509–512. [PubMed: 10521342]
3. Becker RA, Chambers JM AND Wilks AR, 1988 The New S Language Pacific Grove, CA: Wadsworth Brooks Cole.
4. Beckmann CF and Smith SM, 2004 Probabilistic independent component analysis for functional magnetic resonance imaging. IEEE Transactions on Medical Imaging, 23, 137–152. [PubMed: 14964560]
5. Beckmann CF and Smith SM. 2005 Tensorial extensions of independent component analysis for multisubject FMRI analysis. Neuroimage, 25, 294–311. [PubMed: 15734364]
6. Biswal B, Yetkin F, Haughton VM, Hyde JS, 1995 Functional connectivity in the motor cortex of resting human brain using echo-planar MRI. Magnetic resonance in medicine 34(4), 537–541. [PubMed: 8524021]
7. Calhoun V, Adali T, Pearlson G and Pekar J, 2001 A method for making group inferences from functional MRI data using independent component analysis. Human brain mapping, 14, 140–151. [PubMed: 11559959]

8. Chang C, Glover GH, 2010 Time-frequency dynamics of resting-state brain connectivity measured with fMRI. Neuroimage 50(1), 81–98. [PubMed: 20006716]
9. Chang C, Liu Z, Chen MC, Liu X, Duyn JH, 2013, EEG correlates of time-varying BOLD functional connectivity. Neuroimage 72, 227–236. [PubMed: 23376790]
10. Chiang S, Cassese A, Guindani M, Vannucci M, Yeh HJ, Haneef Z and Stern JM, 2016 Time-dependence of Graph Theory Metrics in Functional Connectivity Analysis. NeuroImage 125, 601–615. [PubMed: 26518632]
11. Cox RW, 1996 AFNI: software for analysis and visualization of functional magnetic resonance neuroimages. Computers and Biomedical research 29(3), 162–173. [PubMed: 8812068]
12. Cox RW, 2012 AFNI: what a long strange trip it's been. Neuroimage 62(2), 743–747. [PubMed: 21889996]
13. Cribben I, Haraldsdottir R, Atlas LY, Wager TD, Lindquist MA, 2012 Dynamic connectivity regression: determining state-related changes in brain connectivity. Neuroimage 61(4), 907–920. [PubMed: 22484408]
14. Cribben I, Wager TD, Lindquist MA, 2013 Detecting functional connectivity change points for single-subject fmri data. Frontiers in Computational Neuroscience 7, 143. [PubMed: 24198781]
15. Dyckman KA, Camchong J, Clementz BA, McDowell JE, 2007 An effect of context on saccade-related behavior and brain activity. Neuroimage 36(3), 774–784. [PubMed: 17478104]
16. Erdos P, Renyi A, 1960 On the evolution of random graphs. Publ. Math. Inst. Hung. Acad. Sci 5(1), 17–60.
17. Fox MD, Snyder AZ, Vincent JL, Corbetta M, Van Essen DC, Raichle ME, 2005 The human brain is intrinsically organized into dynamic, anticorrelated functional networks. Proceedings of the National Academy of Sciences of the United States of America 102(27), 9673–9678. [PubMed: 15976020]
18. Friedman J, Hastie T, Tibshirani R, 2008 Sparse inverse covariance estimation with the graphical lasso. Biostatistics 9(3), 432–441. [PubMed: 18079126]
19. Greicius MD, Krasnow B, Reiss AL, Menon V, 2003 Functional connectivity in the resting brain: a network analysis of the default mode hypothesis. Proceedings of the National Academy of Sciences 100(1), 253–258.
20. Guo Y, 2011 A general probabilistic model for group independent component analysis and its estimation methods. Biometrics 67(4), 1532–1542. [PubMed: 21517789]
21. Guo Y, Pagnoni G, 2008 A unified framework for group independent component analysis for multi-subject fMRI data. NeuroImage 42, 1078–1093. [PubMed: 18650105]
22. Handwerker DA, Roopchansingh V, Gonzalez-Castillo J, Bandettini PA, 2012 Periodic changes in fMRI connectivity. Neuroimage 63,1712–1719. [PubMed: 22796990]
23. Hellyer PJ, Shanahan M, Scott G, Wise RJ, Sharp DJ, Leech R, 2014 The control of global brain dynamics: opposing actions of frontoparietal control and default mode networks on attention. Journal of Neuroscience 34(2), 451–461. [PubMed: 24403145]
24. Hindriks R, Adhikari MH, Murayama Y, Ganzetti M, Mantini D, Logothetis NK, Deco G, 2016 Can sliding-window correlations reveal dynamic functional connectivity in resting-state fMRI?. Neuroimage 127, 242–256. [PubMed: 26631813]
25. Huang H, Li J, Sun L, Liu J, Wu T, Chen K, Fleisher A, Reiman E, Ye J, 2009 Learning brain connectivity of Alzheimers disease from neuroimaging data. In Advances in Neural Information Processing Systems, 808–816.
26. Hutchison RM, Womelsdorf T, Gati JS, Everling S, Menon RS, 2013 Resting-state networks show dynamic functional connectivity in awake humans and anesthetized macaques. Hum. Brain Mapp 34(9), 2154–2177. [PubMed: 22438275]
27. Hutchison RM, Womelsdorf T, Allen EA, Bandettini PA, Calhoun VD, Corbetta M, Penna SD, Duyu J, et al., 2013 Dynamic functional connectivity: promise, issues, and interpretations. Neuroimage 80, 360–378. [PubMed: 23707587]
28. Hyvarinen A and Oja E, 2000 Independent component analysis: algorithms and applications. Neural networks 13(4), 411–430. [PubMed: 10946390]

29. Jones DT, Vemuri P, Murphy MC, Gunter JL, Senjem ML, Machulda MM, Przybelski SA, Gregg BE, Kantarci K, Knopman DS, Boeve BF, Petersen RC, Jack CR, Jr., 2012 Non-stationarity in the "resting brain's" modular architecture. PLoS One 7(6):e39731. [PubMed: 22761880]
30. Li X, Lim C, Li K, Guo L, Liu T, 2013 Detecting Brain State Changes via Fiber-Centered Functional Connectivity Analysis. Neuroinformatics 11(2), 193–210. [PubMed: 22941508]
31. Lian Z, Li X, Pan y., Guo X, Chen L, Chen G, Wei Z, Liu T, Zhang J, 2015 Dynamic Bayesian brain network partition and connectivity change point detection, In Computational Advances in Bio and Medical Sciences (ICCABS), 2015 IEEE 5th International Conference on (pp. 1–6). IEEE.
32. Lindquist MA, Xu Y, Nebel MB, Caffo BS, 2014 Evaluating dynamic bivariate correlations in resting-state fMRI: A comparison study and a new approach. Neuroimage 101, 531–546. [PubMed: 24993894]
33. McDowell JE, Dyckman KA, Austin BP, Clementz BA, 2008 Neurophysiology and neuroanatomy of reflexive and volitional saccades: evidence from studies of humans. Brain and cognition 68(3), 255–270. [PubMed: 18835656]
34. Mckeown MJ, Makeig S, Brown GG, Jung T-P, Kindermann SS, Kindermann RS, Bell AJ and Sejnowski TJ (1998). Analysis of fMRI Data by Blind Separation Into Independent Spatial Components. Human Brain Mapping, 6, 160–188. [PubMed: 9673671]
35. Monti RP, Hellyer P, Sharp D, Leech R, Anagnostopoulos C, Montana G, 2014 Estimating time-varying brain connectivity networks from functional MRI time series. NeuroImage 103, 427–443. [PubMed: 25107854]
36. Picard F, Robin S, Lavielle M, Vaisse C, Daudin JJ, 2005 A statistical approach for array CGH data analysis. BMC bioinformatics 6(1), 27. [PubMed: 15705208]
37. Plitt M, Barnes KA, Martin A, 2015 Functional connectivity classification of autism identifies highly predictive brain features but falls short of biomarker standards. NeuroImage: Clinical 7, 359–366. [PubMed: 25685703]
38. Politis DN, Romano JP, 1994 The stationary bootstrap. Journal of the American Statistical association 89(428), 1303–1313.
39. Sakoglu U, Pearlson GD, Kiehl KA, Wang YM, Michael AM, Calhoun VD, 2010 A method for evaluating dynamic functional network connectivity and task-modulation: application to schizophrenia. Magnetic Resonance Materials in Physics, Biology and Medicine 23(5–6), 351–366.
40. Salvador R, Suckling J, Schwarzbauer C, and Bullmore E, 2005 Undirected graphs of frequency-dependent functional connectivity in whole brain networks. Philosophical Transactions of the Royal Society B: Biological Sciences 360(1457), 937–946.
41. Shirer WR, Ryali S, Rykhlevskaia E, Menon V, Greicius MD, 2012 Decoding subject-driven cognitive states with whole-brain connectivity patterns. Cereb. Cortex 22,158 −165. [PubMed: 21616982]
42. Smith SM, Fox PT, Miller KL, Glahn DC, Fox PM, Mackay CE, Filippini N,Watkins KE, Toro R, Laird AR, Beckmann CF, 2009 Correspondence of the brain's functional architecture during activation and rest. Proc. Natl. Acad. Sci. U.S.A 106, 13040–13045. [PubMed: 19620724]
43. Smith SM, Miller KL, Salimi-Khorshidi G, Webster M, Beckmann CF, Nichols TE, Ramsey JD, and Woolrich MW, 2011 Network modelling methods for fmri. Neuroimage 54(2), 875–891. [PubMed: 20817103]
44. Stam CJ, Jones BF, Nolte G, Breakspear M, Scheltens P, 2007 Small-world networks and functional connectivity in Alzheimer's disease. Cerebral cortex 17(1), 92–99. [PubMed: 16452642]
45. Supekar K, Menon V, Rubin D, Musen M, and Greicius MD, 2008 Network analysis of intrinsic functional brain connectivity in alzheimers disease. PLoS Computational Biology 4(6), e1000100. [PubMed: 18584043]
46. Tagliazucchi E, Von Wegner F, Morzelewski A, Brodbeck V, Laufs H, 2012 Dynamic BOLD functional connectivity in humans and its electrophysiological correlates. Frontiers in human neuroscience 6, 339. [PubMed: 23293596]

47. Tibshirani R, 1996 Regression shrinkage and selection via the lasso. Journal of the Royal Statistical Society Series B (Methodological), 267–288.

48. Tibshirani R, Saunders M, Rosset S, Zhu J, Knight K, 2005 Sparsity and smoothness via the fused lasso. Journal of the Royal Statistical Society: Series B (Statistical Methodology) 67(1), 91–108.

49. Tibshirani R, Wang P, 2008 Spatial smoothing and hot spot detection for CGH data using the fused lasso. Biostatistics 9(1), 18–29. [PubMed: 17513312]

50. Thompson G, Magnuson M, Merritt M, Schwarb H, Pan W, McKinley A, Tripp L, Schumacher E, Keilholz S, 2013 Short time windows of correlation between large scale functional brain networks predict vigilance intra-individually and inter-individually. Hum Brain Mapping 34(12), 3280–3298.

51. Vert J and Bleakley K (2010), “Fast detection of multiple change-points shared by many signals using group LARS,” Advances in Neural Information Processing Systems, 23, 2343–2351.

52. Wang K, Liang M, Wang L, Tian L, Zhang X, Li K, Jiang T, 2007 Altered functional connectivity in early Alzheimer’s disease: a resting?state fMRI study. Human brain mapping, 28(10), 967–978. [PubMed: 17133390]

53. Wang Y, Jian K, Kemmer PB, and Guo Y, 2016 An Efficient and Reliable Statistical Method for Estimating Functional Connectivity in Large Scale Brain Networks Using Partial Correlation. Frontiers in neuroscience, 10.

54. Watts DJ, Strogatz SH, 1998 Collective dynamics of small-world networks. Nature 393(6684), 440–442. [PubMed: 9623998]

55. Woodward ND, Cascio CJ, 2015 Resting-state functional connectivity in psychiatric disorders. JAMA Psychiatry 72(8), 743–744. [PubMed: 26061674]

56. Xu Y, Lindquist MA, 2015 Dynamic connectivity detection: an algorithm for determining functional connectivity change points in fMRI data. Frontiers in neuroscience, 9.

57. Yuan M and Lin Y, 2006 Model selection and estimation in regression with grouped variables. Journal of the Royal Statistical Society, Series B, 68(1):4967.

Algorithm I: Estimation of the Number of Change Points

1. Compute a value of penalty parameter λ for fused lasso model (2).

1.1 Apply lowess independently to all the time series of pairwise correlations, under a small value of the fraction parameters to avoid overfttting.

1.2 Compute the differences $\delta_{kt} = \bar{\rho}_{kt} - \bar{\rho}_{k,t+1}, t = 1, \ldots, T-1$ where $\bar{\rho}_k = (\bar{\rho}_{k1}, \ldots, \bar{\rho}_{kT})$ denotes the lowess ftt for the k-th time series.

1.3 For each ftrst order difference, compute the median of $(\delta_{kt}, \ldots, \delta_{kT})$ as μ_k.

1.4 For each ftrst order difference, compute $\{|\delta_{k1} - \mu_k|, \ldots, |\delta_{kT} - \mu_k|\}$

1.5 Compute the median of the differences $\{|\delta_{k1} - \mu_k|, \ldots, |\delta_{kT} - \mu_k|\} as \Delta_k$

1.6 Compute the penalty parameter as $\lambda = \min_{k=1,\ldots,p}\left\{2\Delta_k + \sum_{t=1}^{T-1}|\delta_{kt}|1(|\delta_{kt}| > 4\Delta_k)\right\}$.

2. Fit the fused lasso model (2) under the chosen value of λ in step 1, and compute an initial set of $Kmax$ change points denoted as $\boldsymbol{\tau}^*_{Kmax}$.

3. Screen out false change points detected in step 2

3.1 Compute normalized scores $J_k = \frac{SSE(Kmax) - SSE(K)}{SSE(Kmax) - SSE(1)}(Kmax - 1) + 1$, where $J(1) = Kmax, J(Kmax) = 1$.

3.2 Compute discrete second derivatives as $\nabla_k = J_{k-1} - 2J_k + J_{k+1}$.

3.3 Choose the final subset of K time points from the original set of change points $\boldsymbol{\tau}^*_{Kmax}$ such that $K = \max\{1 < k < Kmax: \nabla_k > 0.5\}$.

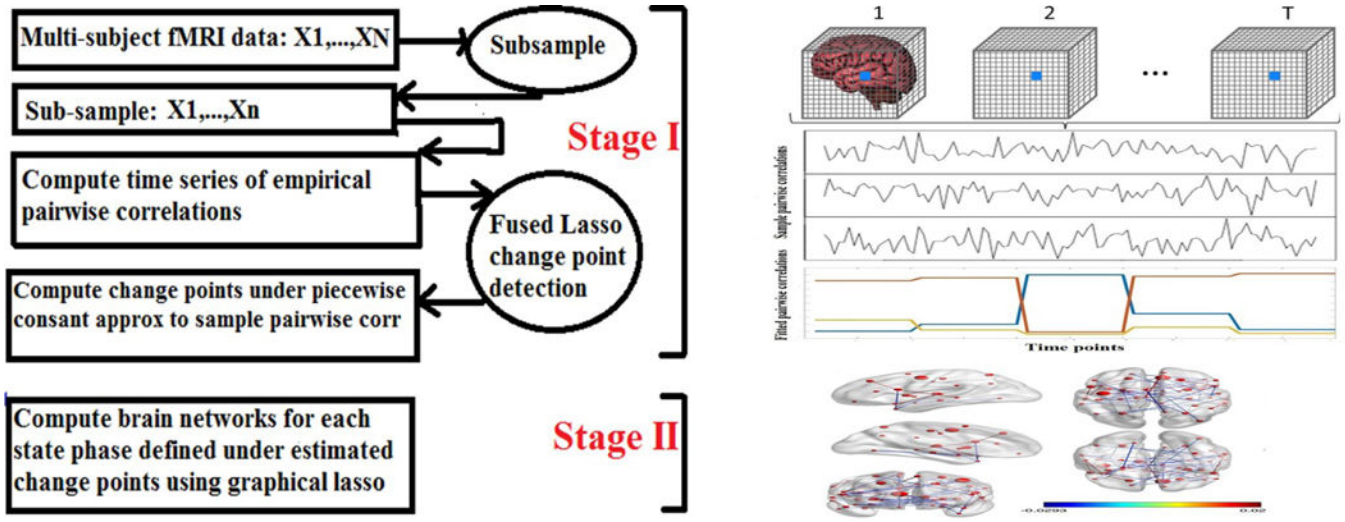

Figure 1:

A visual depiction of the two stage approach. The multi-subject fMRI data is first subsampled, and this sub-sample is used to compute a group level connectivity metric (ρ) at each time point. Subsequently, a fused lasso approach is applied to approximate the time series of the connectivity metric using a piecewise constant function, which automatically detects change points and divides the length of the scanning session into distinct state phases. This process is repeated for multiple sub-samples in order to diminish the influence of aberrant subjects on change point estimation, and those change points which show up most frequently across these subsamples are chosen as the time points where functional connectivity changes occur. In the second stage, a graphical lasso approach is applied independently to the time scans in each state phase to obtain the corresponding brain functional networks. The collection of these brain networks across state phases represents the time varying brain functional connectivity.

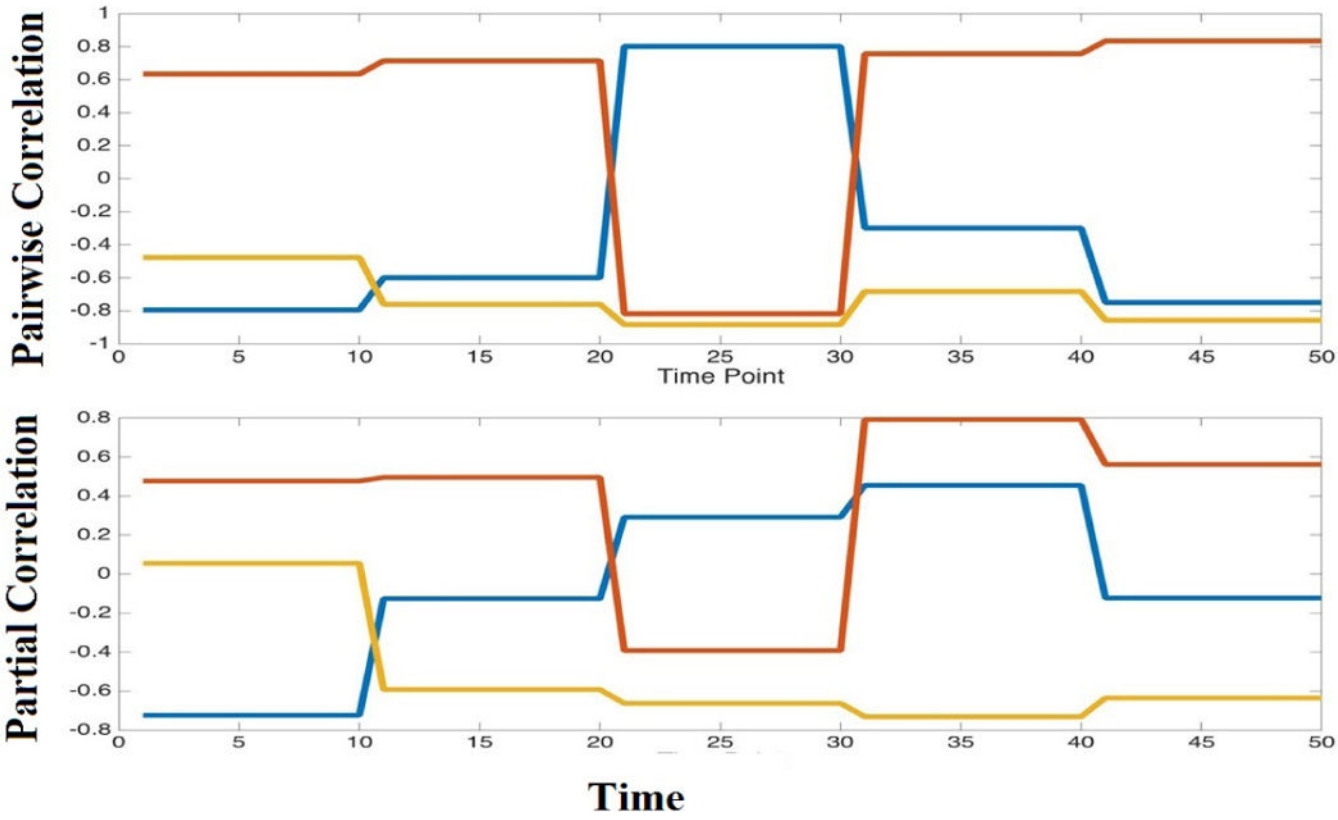

Figure 2:

Toy example involving 3 regions and 50 time points, showing changes in pair-wise correlations (top) and corresponding partial correlations (below) across time points when the data is generated under a mixture model with multiple change points. Each component of the mixture model follows a Gaussian distribution with mean zero and a distinct inverse covariance matrix quantifying the functional associations corresponding to time intervals 1 −10,11−20,21−30,31−40, and 41 −50. The time varying network illustrated in the above diagram has 5 state phases, and is characterized by piece-wise constant pair-wise and partial correlations having the exact same change points.

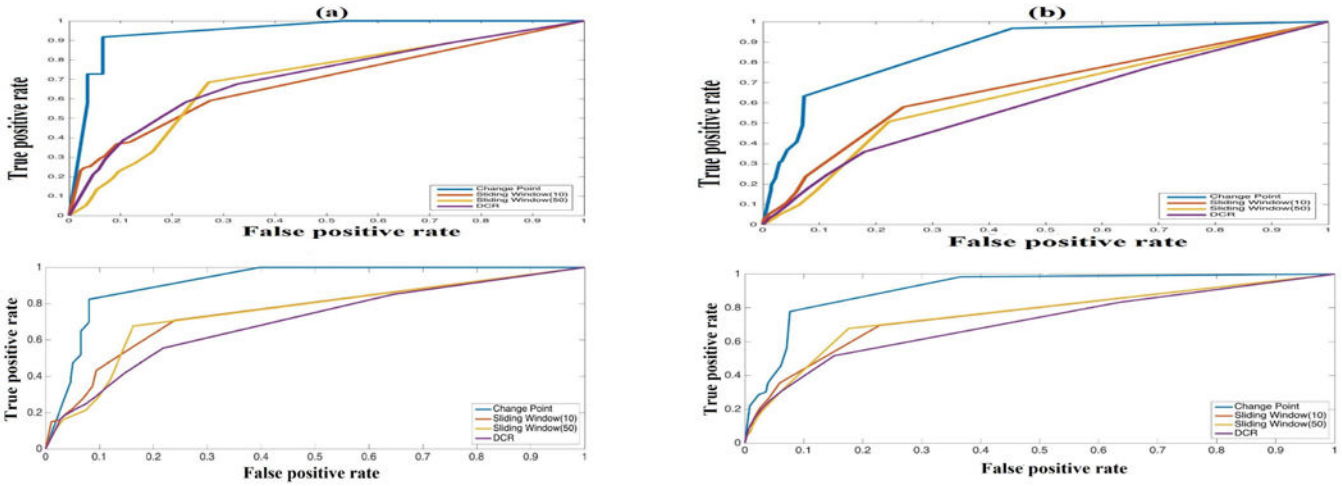

Figure 3:

The receiver operating characteristic (ROC) curves, which plot the sensitivity versus the false positive rate, are presented for the first four simulation scenarios. The ROC curves for the proposed change point approach, the dynamic connectivity regression approach, and the sliding window approach with window lengths 10 and 50 are depicted with blue, magenta, red, and orange solid lines respectively.

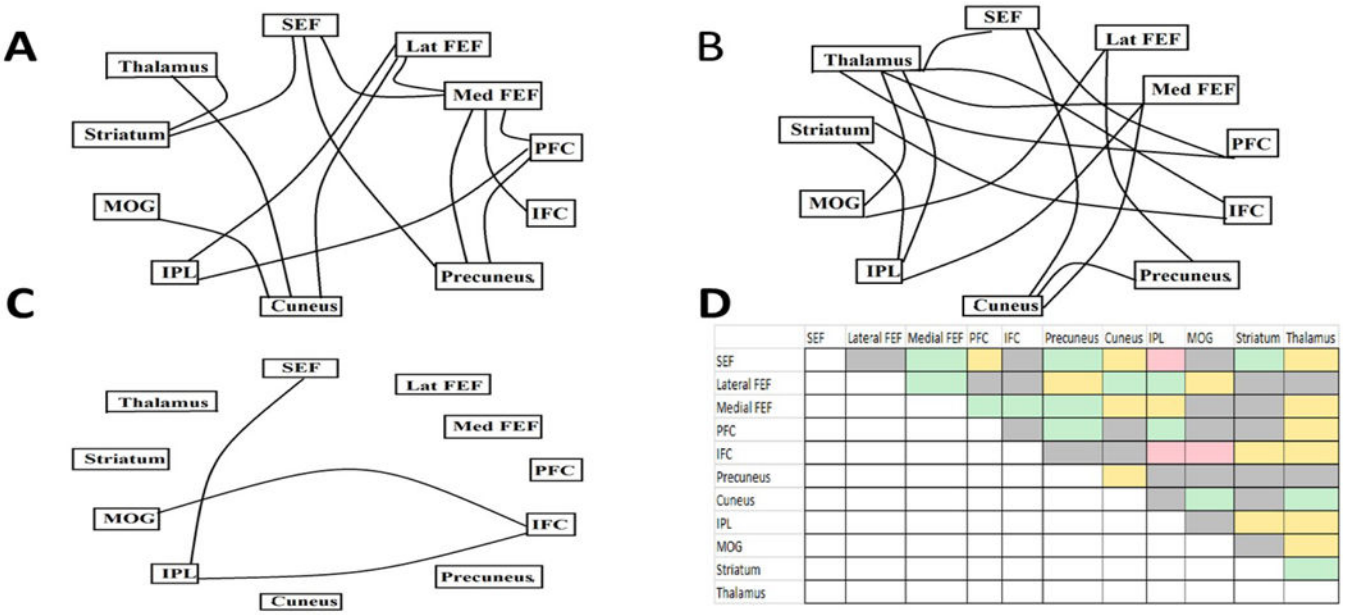

Figure 4:

A visual depiction of functional connectivity in the saccade trial. The Figures display connections which are present in both pro-saccade and fixation (Figure A), connections which are present in pro-saccade blocks only (Figure B), and connections which are present in fixation blocks only (Figure C). Figure D provides a color coded table which indicates a connection present in both pro-saccade and fixation in green, connection appearing only in pro-saccades in yellow, connections appearing only in fixation in pink, and connections which do not appear in either blocks in gray.

Table 1:

Simulation results. The first column reports simulation scenarios described in Section 3.1.1, the second and third columns denote the number of nodes and time points respectively, the fourth column (CP) reports the proportion of change points estimated accurately, the fifth and sixth columns (SE and SP) report the average sensitivity and specificity under the proposed approach. Columns 7–9 report the proportion of change points detected under DCR, and the corresponding sensitivity and specificity. The last four columns report sensitivity and specificity under the sliding window approach with window lengths 10 and 50. Note that the sliding window approach does not admit change point detection. All results are averaged over 100 replicates.

			CCPD			DCR			SL(10)		SL(50)	
Simulation setup	**p**	**T**	**CP**	**SE**	**SP**	**CP**	**SE**	**SP**	**SE**	**SP**	**SE**	**SP**
random	10	200	1	0.86	0.96	0.16	0.21	0.89	0.73	0.94	0.65	0.88
random	20	200	1	0.91	0.95	0.18	0.23	0.87	0.39	0.97	0.33	0.93
random	10	300	1	0.87	0.93	0.13	0.23	0.88	0.64	0.93	0.60	0.89
random	20	300	1	0.91	0.91	0.10	0.20	0.87	0.44	0.97	0.43	0.94
random + mean shift	10	200	1	0.92	0.99	0.05	0.09	0.95	0.78	0.83	0.94	0.30
random + mean shift	20	200	1	0.91	0.95	0.16	0.11	0.96	0.40	0.90	0.68	0.49
random + mean shift	10	300	1	0.85	0.98	0.03	0.08	0.96	0.52	0.84	0.79	0.36
random + mean shift	20	300	1	0.91	0.97	0.09	0.09	0.96	0.41	0.93	0.62	0.64
random + spikes	10	200	1	0.86	0.96	0.005	0.08	0.96	0.55	0.89	0.67	0.56
random + spikes	20	200	1	0.92	0.94	0.033	0.11	0.94	0.44	0.98	0.36	0.91
random + spikes	10	300	1	0.87	0.94	0.002	0.09	0.96	0.71	0.94	0.63	0.88
random + spikes	20	300	1	0.91	0.91	0.005	0.08	0.95	0.32	0.97	0.33	0.92
Erdos-Renyi	10	200	1	0.93	0.99	0.12	0.25	0.93	0.63	0.93	0.54	0.86
Erdos-Renyi	20	200	1	0.88	0.99	0.06	0.22	0.94	0.54	0.98	0.42	0.96
Erdos-Renyi	10	300	1	0.93	0.99	0.11	0.22	0.93	0.63	0.95	0.60	0.91
Erdos-Renyi	20	300	1	0.88	0.99	0.16	0.18	0.89	0.60	0.98	0.63	0.95
small world	10	200	1	0.87	0.99	0.11	0.21	0.94	0.50	0.93	0.56	0.87
small world	20	200	1	0.93	0.99	0.084	0.15	0.95	0.43	0.98	0.34	0.95
small world	10	300	1	0.85	0.99	0.017	0.18	0.97	0.71	0.92	0.66	0.87
small world	20	300	1	0.91	0.99	0.022	0.19	0.93	0.56	0.98	0.53	0.96
scale free	10	200	1	0.87	0.99	0.1611	0.20	0.92	0.38	0.93	0.44	0.85
scale free	20	200	1	0.95	0.99	0.0583	0.14	0.92	0.38	0.98	0.43	0.94
scale free	10	300	1	0.92	0.99	0.0278	0.17	0.94	0.62	0.90	0.69	0.82

Simulation setup	p	T	CCPD			DCR			SL(10)			SL(50)		
			CP	SE	SP	CP	SE	SP	SE	SP		SE	SP	
scale free	20	300	1	0.89	0.99	0.0222	0.16	0.95	0.45	0.98		0.46	0.94	

Table 2:

Computation time reported in seconds under the proposed approach. Here N, P and T are number of subjects, number of nodes in the network, and time points.

Simulation	N	P	T	time (in secs)
1	60	10	200	14.34
2	60	20	200	60.35
3	60	10	300	20.01
4	60	20	300	67.89
5	60	50	300	215.44